Prolonging qubit coherence: dynamical decoupling schemes studied in a Penning ion trap[*]

Hermann Uys[a,b], Michael J. Biercuk[a,c], Aaron P. VanDevender[a], Nobuyasu Shiga[a,d], Wayne M. Itano[a], John J. Bollinger[a]

[a]National Institute of Standards and Technology, 325 Broadway, Boulder, CO, 80305
[b]Council for Scientific and Industrial Research, Brummeria, Pretoria, South Africa
[c]also Georgia Institute of Technology, Atlanta, Georgia
[d]Present address: NICT, Tokyo, Japan

January 2, 2009

ABSTRACT

We present a study of dynamical decoupling schemes for the suppression of phase errors from various noise environments using ions in a Penning trap as a model ensemble of qubits. By injecting frequency noise we demonstrate that in an ohmic noise spectrum with a sharp, high-frequency cutoff the recently proposed UDD decoupling sequence gives noise suppression superior to the traditional CPMG technique. Under only the influence of ambient magnetic field fluctuations with a $1/\omega^4$ power spectrum, we find little benefit from using the UDD sequence, consistent with theoretical predictions for dynamical decoupling performance in the presence of noise spectra with soft cutoffs. Finally, we implement an optimization algorithm using measurement feedback, demonstrating that local optimization of dynamical decoupling can further lead to significant gains in error suppression over known sequences.

1. INTRODUCTION

Reliable application of quantum phenomena often hinges on the ability to successfully combat the deleterious effects of decoherence. Decoherence processes can broadly be characterized into two classes: dephasing (so-called T_2 processes) which are generally reversible, and energy relaxation (T_1 processes) which are generally irreversible. The nuclear magnetic resonance (NMR) spectroscopy community developed effective protocols for suppressing phase errors starting over half a century ago.[1] These protocols are commonly referred to as spin-echo techniques or dynamical decoupling.

It is natural to ask whether these techniques can be employed in the context of quantum information processing, which generally has far more stringent fidelity requirements than NMR. For example, the fault-tolerant threshold for quantum computing is predicted to require an intrinsic qubit error rate of the order $10^{-3} \sim 10^{-6}$.[2,3] Indeed, recent theoretical studies[4–9] have predicted that appropriate adaptation of well known dynamical decoupling techniques can lead to dramatically improved fidelities in certain relevant noise environments, thus providing a resource efficient alternative to brute-force quantum error-correction code concatenation.

In this proceeding we report on a study of dynamical decoupling schemes applied to ions in a Penning trap. Our system serves as a model for qubits in a variety of physical systems, as we are able to engineer the noise environment to simulate those of other physical systems. We compare the performance of traditional NMR techniques[10] to a dynamical decoupling scheme recently proposed by Uhrig,[7,8] so-called Uhrig dynamical decoupling (UDD), illustrating the latter's superiority in certain noise environments. Although originally developed in the context of a spin-boson model, this scheme has been shown to have universal applicability[11] over a wide range of noise models. We further introduce sequences optimized by either simulation or measurement feedback that demonstrate even greater gains in fidelity over standard sequences.

The rest of this paper is structured as follows. In section 2 we lay the theoretical ground work by discussing the physical principles underlying dynamical decoupling and providing the relevant mathematical description. Section 3 describes our experimental setup, while results comparing the above mentioned schemes are shown in section 4. Section 5 discusses our optimization technique and results, and a conclusion is presented in section 6.

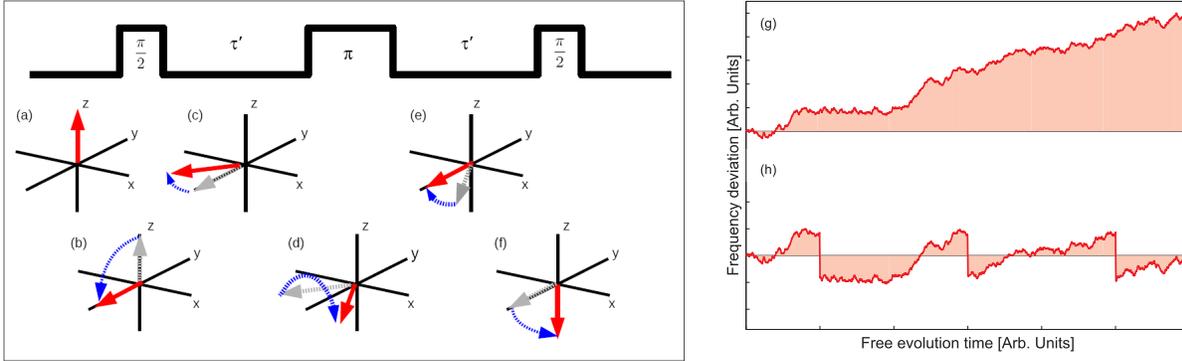[*] Work of the U.S. government. Not subject to U.S. copyright.

Figure 1. Left - A spin echo pulse sequence rotates the qubit as shown in (b), (d), and (f), thereby partially cancelling phase errors that occur during the inter-pulse delays (c) and (e). Right - (g) The net phase accumulated by a qubit due to a random noise field is proportional to the integral over the instantaneous frequency deviation, see Eq. (4), caused by that field, and represented by the shaded area under the solid curve. A dynamical decoupling sequence, in this case 3π-pulse CPMG, can reduce the phase error as schematically shown in (h) where the positive and negative contributions to the area cancel.

2. DYNAMICAL DECOUPLING

2.1 Spin Echo

We consider the time evolution of an ensemble of two-level systems (qubits) under the influence of a random classical noise field that causes an instantaneous deviation in frequency, $\beta(t)$, from the resonant qubit frequency Ω. The dynamics of each qubit are governed by the following Hamiltonian:

$$\hat{H} = \frac{1}{2}\hbar\left[\Omega + \beta(t)\right]\hat{\sigma}_z, \tag{1}$$

where $\hat{\sigma}_j$ the j'th Pauli spin matrix. A heuristic representation of a typical spin echo experiment is shown in Fig. 1. The qubit is firstly prepared in the "up" state $|\uparrow\rangle$, Fig. 1(a), pointing along the quantization (z) axis. A $\pi/2$-pulse then rotates the spin around the x-axis into a superposition state

$$|\psi(t=0)\rangle = (|\uparrow\rangle + i|\downarrow\rangle)/\sqrt{2} \tag{2}$$

pointing along the y-axis, Fig. 1b. In a frame rotating with the frequency Ω, the qubit would remain stationary along the y-axis, were it not for the noise field. However, modulation of the qubit splitting away from resonance due to the noise field during a delay of length τ' will cause a rotation about the z-axis, as shown in Fig. 1(c). A π-pulse is applied next, rotating the qubit around y-axis by 180°, Fig. 1(d). If τ' is short compared to the correlation time characterizing the noise field, then the noise in a subsequent delay, again of length τ', will be strongly correlated to that in the initial delay, causing the qubit to approximately rotate back onto the y-axis, Fig. 1(e). A final $\pi/2$-pulse is applied, Fig. 1(f), after which a projective measurement (on the ensemble) will determine the relative populations of qubits in the up- or down-states. If the realignment of qubits with the y-axis due to the echo pulse sequence was perfect, all qubits will end in the down-state, while any misalignment, i.e., a phase-control error, will lead to some fraction of the population in the up-state. When τ' becomes long compared to the correlation time of the noise-field, the misalignment can produce large phase excursions so that the qubit can assume any position in the xy-plane, and consequently have an equal probability of ending in the up- or down-state after the final $\pi/2$-pulse.

This simple, but powerful, technique was first implemented by E.L. Hahn in 1950,[1] when he observed a reappearance of the NMR signal at the end of the second delay τ', hence the name "spin-echo". In essence one exploits the noise field to cancel its unwanted effect!

A straightforward extension of this technique is the so-called Carl-Purcell-Meiboom-Gill (CPMG)[10] method, which, after the initial delay of τ', concatenates a succession of π-pulses separated by delays $2\tau'$, ending with another τ' delay, thus cancelling out successive deviations of the qubit from the y-axis.

To describe the above experiments theoretically we follow closely the work in.[7–9] Assume an arbitrary noise field and a spin-echo sequence during which n instantaneous π-pulses, $\Pi_y = e^{i\frac{\pi}{2}\hat{\sigma}_y} = i\hat{\sigma}_y$, are applied at fractions δ_j, $j = 1, 2, ...n$, of the total free-evolution time τ. In this case the time evolution of the initial state, Eq. (2), is given

$$|\psi(t)\rangle = e^{-\frac{i}{2}\hat{\sigma}_z \int_{\delta_n \tau}^{\delta_{n+1}\tau} \beta(t')dt'} ... e^{-\frac{i}{2}\hat{\sigma}_z \int_{\delta_2 \tau}^{\delta_3 \tau} \beta(t')dt'} \Pi_y e^{-\frac{i}{2}\hat{\sigma}_z \int_{\delta_1 \tau}^{\delta_2 \tau} \beta(t')dt'} \Pi_y e^{-\frac{i}{2}\hat{\sigma}_z \int_{\delta_0 \tau}^{\delta_1 \tau} \beta(t')dt'} (|\uparrow\rangle + i|\downarrow\rangle)/\sqrt{2}. \quad (3)$$

In the absence of π-pulses the total random phase that the qubit accumulates is given by $\phi(t) = \int_0^\tau \beta(t)dt$. After commuting every other operator Π_y to the left once in Eq. (3), we see that due to the π-pulses this random phase becomes instead

$$\phi(t) = (-1)^n \int_{\delta_n \tau}^{\delta_{n+1}\tau} \beta(t')dt'... - \int_{\delta_2 \tau}^{\delta_3 \tau} \beta(t')dt' + \int_{\delta_1 \tau}^{\delta_2 \tau} \beta(t')dt' - \int_{\delta_0 \tau}^{\delta_1 \tau} \beta(t')dt'. \quad (4)$$

This is schematically represented on the right in Fig. 1(g)-(h) for a three pulse CPMG sequence, demonstrating that the net random phase can be expected to be reduced relative to simple free evolution. After carrying out the operator algebra, one finds the following time dependence for the expectation value of $\hat{\sigma}_y$, which we use as a measure of coherence:

$$W(\tau) = |\overline{\langle\sigma_y(\tau)\rangle}| = e^{-2\chi(\tau)}, \quad (5)$$

where $\chi(t)$ is the coherence integral,

$$\chi(\tau) = \frac{1}{\pi} \int_0^\infty S(\omega) \frac{F(\omega\tau)}{\omega^2} d\omega. \quad (6)$$

In Eq. (5) the angle brackets indicate the quantum mechanical expectation value and the over-line an ensemble average. $S(\omega)$ in Eq. (6) is the power spectral density of the noise field, ω the angular frequency, and $F(\omega\tau)$ is a filter function function dependent on the total free-evolution time, τ, and the times at which the n π-pulses are applied

$$F(\omega\tau) = \left| 1 + (-1)^{n+1} e^{i\omega\tau} + 2\sum_{j=1}^n (-1)^j e^{i\omega\delta_j \tau} \right|^2. \quad (7)$$

Tailoring the filter function by choosing appropriate pulse sequences can lead to enhanced suppression of dephasing.

2.2 Uhrig Dynamical Decoupling

The dynamical decoupling techniques described so far, of which Hahn spin echo is the simplest form, were developed in the context of NMR. As mentioned in the introduction, recent theoretical results suggest[4–9] that appropriate choices of the inter-pulse delays, given a fixed total free-evolution time τ, can potentially adapt these techniques to the stringent fidelity requirements of quantum information processing. As a benchmark, we will use in this paper the analytically optimized UDD scheme.[7,8] To our knowledge this is (for a fixed number of pulses) the most promising scheme for suppression of phase errors out of many candidates currently discussed in the literature including CPMG, periodic dynamical decoupling and concatenated dynamical decoupling.[9] The UDD scheme consists of applying π-pulses at fractions of the total free-evolution time given by

$$\delta_j = \sin^2\left[\pi j/(2n+2)\right]. \quad (8)$$

This sequence is arrived at by enforcing the condition that all of the first n derivatives of the filter function (evaluated at $\omega\tau = 0$) for an n-pulse sequence should vanish. Looking at Eq. (6) one sees that this would have the effect of strongly suppressing noise in the frequency range where terms of order $n + 1$ and higher in an expansion of the filter function in $\omega\tau$ are neglegible. Uhrig showed[8] that in systems where the noise spectrum is characterized by a sharp cutoff, such as the Ohmic spectrum associated with a spin-boson model describing semiconductor quantum dots, the error-suppression using the UDD sequence can outperform that due to CPMG by orders of magnitude. Figure 2 demonstrates this for a 6 π-pulse sequence and an ohmic spectrum (using
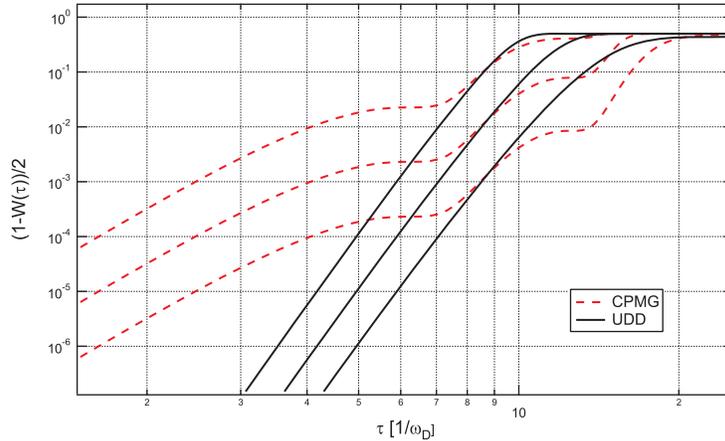
Figure 2. Numerical simulations comparing error suppression by CPMG (dashed lines) vs. UDD (solid lines) for an ohmic power spectrum, $S(\omega) = \alpha\omega$, with a sharp high-frequency cutoff at ω_D and $\alpha = 10^{-1}, 10^{-2}$ and 10^{-3}. The lowest curve in each set (CPMG and UDD) corresponds to the weakest α.
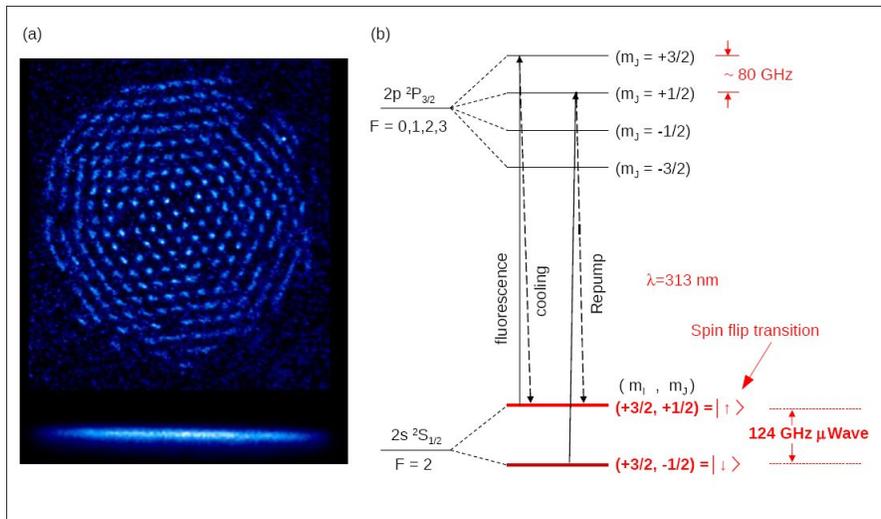

Figure 3. (a) Fluorescence image of a single crystal plane of ions as seen from the top (rotation axis normal to the image plane) and the side (bottom image). (b) Level structure of $^9Be^+$. In the 4.5 T magnetic field m_I and m_J are good (although approximate) quantum numbers. For simplicity we only show the $m_I = +3/2$ states.

Eqs. (5)-(7)), comparing the coherence due to CPMG to that due to UDD at different noise strengths. As expected the coherence decreases for increasing noise strength. Note that at each noise strength there exists a crossing point, to shorter times of which UDD exhibits superior error suppression.

As we will see below, careful numerical or experimental fine-tuning of the pulse-timings can lead to equally dramatic gains in error suppression over the UDD sequence.

3. ION CRYSTALS IN A PENNING TRAP – A MODEL QUBIT SYSTEM

We use $^9Be^+$ ions in a Penning trap as a model qubit system to study various dynamical decoupling schemes. The trap uses a strong, uniform magnetic field (4.5 T in this work) and static electric fields to confine ions. The capabilities of our trap have been discussed in detail elsewhere[12] and here we present only a brief summary. A few hundred to a few thousand ions are trapped and Doppler laser-cooled to ~ 1 mK. Due to $\mathbf{E} \times \mathbf{B}$ drift, an ion cloud in a Penning trap rotates. The rotation frequency of the cloud, in this study approximately $\omega_r/2\pi \sim 20$ kHz, determines the overall shape of the cloud (varying from pancake to cigar shaped), and can be controlled by

six electrodes generating a rotating dipole electric field. The trap is operated in a regime where the ions in the cloud form a rigidly rotating ion crystal consisting of a single or a few crystal planes with a typical ion spacing of $\sim 10\ \mu$m. A fluorescence image of such a crystal is shown in Fig. 3(a).

Figure 3(b) illustrates the relevant ^{9}Be$^+$ energy levels. The $2\mathrm{s}\,^2\mathrm{S}_{1/2}|m_I = 3/2, m_J = -1/2\rangle = |\downarrow\rangle \longrightarrow |m_I = 3/2, m_J = +1/2\rangle = |\uparrow\rangle$ spin-flip transition serves as our qubit, and has a ~ 124 GHz splitting in the 4.5 T magnetic field provided by a superconducting magnet. Rotations of the qubit are induced by injecting a microwave field into the bore of the superconducting magnet. The microwave coupling produces a Rabi flopping π-pulse time of 185 μs, while microwave power fluctuations of 1 part in 10^3 give a Rabi-decay time of $20 \sim 40$ ms. The Ramsey free-precession decay time due to ambient magnetic field fluctuations is ~ 1 ms.

Preparation into the $|\uparrow\rangle$ state occurs via a repump laser driving the $2\mathrm{s}\,^2\mathrm{S}_{1/2}|m_I = 3/2, m_J = -1/2\rangle \longrightarrow 2\mathrm{p}\,^2\mathrm{P}_{1/2}$ $|m_I = 3/2, m_J = +3/2\rangle$ transition, while the $2\mathrm{s}\,^2\mathrm{S}_{1/2}|m_I = 3/2, m_J = +1/2\rangle \longrightarrow 2\mathrm{p}\,^2\mathrm{P}_{3/2}|m_I = 3/2, m_J = +3/2\rangle$ cycling transition is used for Doppler cooling and fluorescence detection of the population of ions in the $|\uparrow\rangle$ state. In the context of the discussion in section II(A), phase errors in rotation of the qubit relative to the y-axis during a decoupling sequence are manifested as fluorescence counts due to a finite number of ions ending in the $|\uparrow\rangle$ state after the final $\pi/2$-pulse. On the other hand, we should observe zero counts for perfect realignment since ions in the $|\downarrow\rangle$ state do not fluoresce in the cooling light. The count rate directly after a dynamical decoupling sequence, normalized to the count rate directly before the sequence is given by $(1 - W(\tau))/2$, see Eq. (5).

4. RESULTS

4.1 Ambient Noise

As discussed in,[8] the qubit state evolution under noise filtration by a given dynamical decoupling sequence depends strongly on the noise spectrum. We measure the ambient magnetic field fluctuations, the dominant noise source in our system, using a shim coil wound around the room temperature bore of the magnet. Figure 4(c) illustrates that this spectrum has an approximate $1/\omega^4$ dependence with some strong spurs. We observe the overall strength of the spectrum to drift on a day-to-day basis and also see fluctuations in the height of the peak at ~ 153 Hz relative to other features in the spectrum. Figure 4(a)-(b) compares the performance of CPMG (squares) to UDD (circles) for four (a) and eight (b) π-pulse sequences. Each datum corresponds to fifty runs of the experiment at a fixed total free-evolution time. As expected, the total coherent free-evolution time increases with the number of π-pulses. The coherence times of both the CPMG and UDD sequences in the presence of the ambient magnetic field noise are comparable, which is consistent with theoretical predictions for noise spectra with soft cutoffs.[8] The solid lines in Figure 4 result from fits to the data using the noise spectrum in Fig. 4(c) and Eqs. (5)-(7) modified to account for the finite length of the π-pulses, as will be described below. In these fits we used two free parameters, namely the overall noise strength and the relative strength of the peak at 153 Hz.

4.2 Injected Noise

The Uhrig sequence is most effective in noise environments with sharp high-frequency cutoffs. To demonstrate the gains in fidelity that may be reached using the UDD sequence under those conditions, we create artificial noise spectra by applying noisy frequency modulation to the reference frequency of our microwave phase-lock-loop. In a frame rotating at the qubit resonance frequency Ω, this approach is indistinguishable from noisy amplitude fluctuations of the ambient magnetic field, which in turn modulate the qubit energy splitting through the Zeeman effect.

A particular noise spectrum is designed by numerically summing a discrete set of frequency components up to a high-frequency cutoff, each component being weighted by the strength of the desired spectrum at that frequency, and having a random phase evenly distributed over the interval $[0, 2\pi]$. A synthesized function generator is programmed to output the resulting time trace as a modulated voltage waveform, which is connected to the external frequency modulation port of a frequency synthesizer that generates the reference frequency for the microwave phase-lock-loop.

Our ability to measure deviations of the ^{9}Be$^+$ state vector from full coherence is currently limited by background counts due to laser light scattered off the trap electrodes. Specifically, we are unable to distinguish between all the ions ending up in the dark state at the end of an echo sequence and 99.5 % ending up in the dark
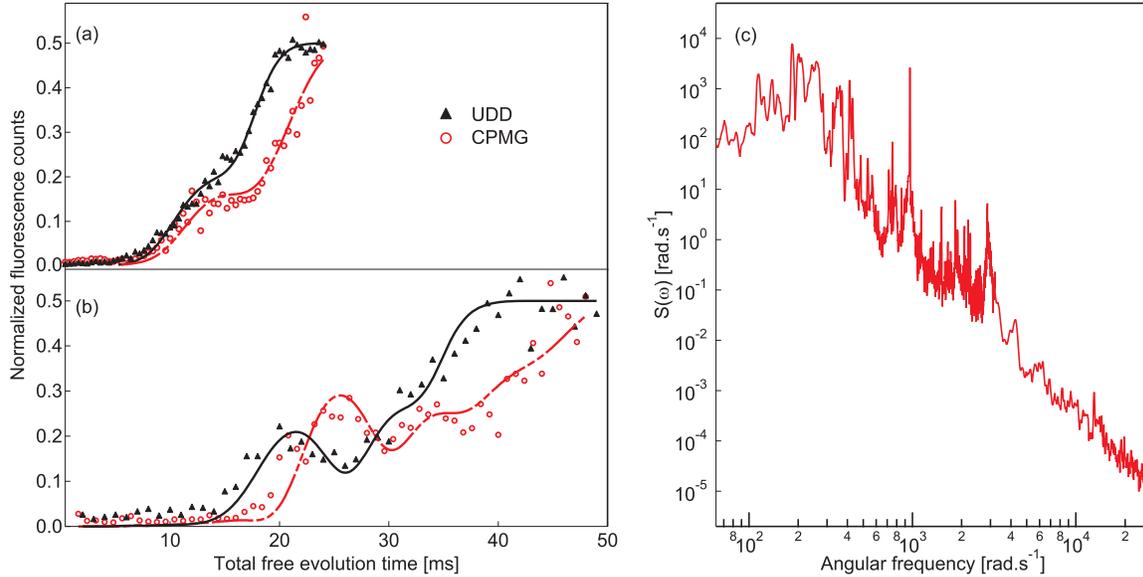
Figure 4. (a) Four and (b) eight π-pulse CPMG (open circles) vs. UDD (black triangles). Here zero fluorescence counts correspond to perfect coherence, while a normalized count rate of 0.5 corresponds to complete loss of coherence. (c) The power spectrum of ambient magnetic field fluctuations in our system.

state. We are consequently limited to studying dynamical-decoupling in a fairly low-fidelity regime. As seen in Fig. 2, however, the crossing point between regions where UDD has stronger error suppression than CPMG shifts to lower fidelity regimes for higher noise strengths. Therefore, by injecting noise of sufficiently high strength we are able to observe the predicted improvements in the low-fidelity regime. This is illustrated in Fig. 5(a) where we compare the performance of CPMG versus UDD under the influence of an ohmic noise spectrum, $S(\omega) = \alpha\omega$, with a cutoff near 500 Hz. We see that in this case UDD (black triangles) gives stronger noise suppression than CPMG (open circles) at most times up to the crossing point around $\tau = 2.6$. The solid lines again represent fits of Eq. (5) to the data. At the earliest times we have poorer agreement with the theoretical predictions, because in these fits we do not take into account the detection threshold discussed above. The threshold is indicated by the horizontal dashed line in Fig. 5(a).

In our implementation the noise was turned off during application of the π-pulses in order to preserve the pulse fidelity. This more closely corresponds to the commonly used theoretical idealization of instantaneous π-pulses in that there is negligible accumulation of random phase during application of the π-pulse. To obtain fits of good quality to our data, it was, however, essential to account for the noise directly before each π-pulse becoming slightly decorrelated from that directly after the pulse due to the finite pulse length. This is done by assuming that the δ_j's in Eq. (3) represent the center of each π-pulse, so that each upper integration limit, in that equation, differs from the lower integration limit of the next phase factor by τ_π, the length of a π-pulse. This assumption introduces a factor $\cos(\omega\tau_\pi/2)$ in the sum on the right in the filter function Eq. (7). It is equivalent to the lowest-order approximation of an expansion of the π-pulse operator in the presence of noise, $e^{-i\int_0^{\frac{\pi}{\gamma 2}}(-\gamma\hat{\sigma}_y+\beta(t)\hat{\sigma}_z)dt}$, in the parameter $2\int_0^{\frac{\pi}{\gamma 2}}\beta(t)dt/\pi$, which is typically $\ll 1$.

5. LOCALLY OPTIMIZED DYNAMICAL DECOUPLING

We now show that using unconstrained optimization one can achieve significant improvements in fidelity over that obtained with UDD, in both the high- and low-fidelity regimes.

Our approach consists of choosing a fixed total free-evolution time, τ, and varying the relative inter-pulse spacings using the Nelder-Mead simplex method[13] to search for a sequence giving a minimum error at that τ. This may be thought of as a locally optimized dynamical decoupling scheme (LODD). To obtain such sequences by
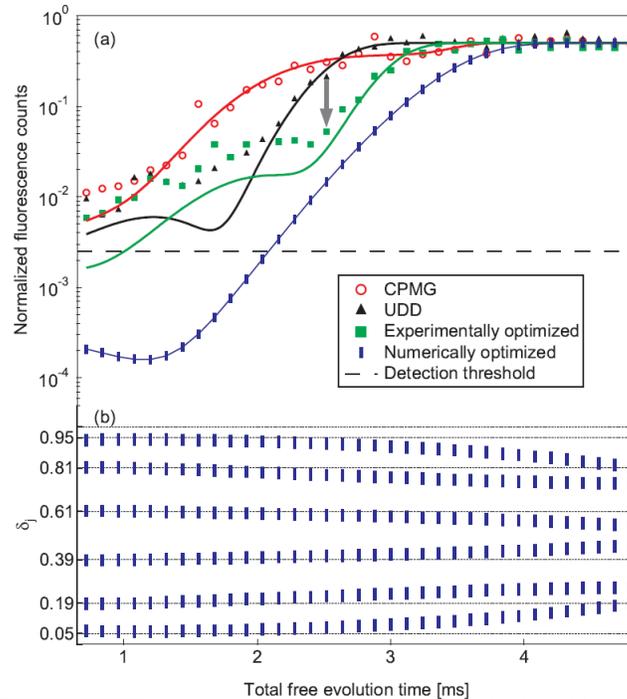
Figure 5. (a) Comparison of 6π-pulse CPMG (open circles), UDD (black triangles) and a sequence optimized via measurement feedback (green squares) at a free evolution time of $\tau = 2.4$ ms. The gray arrow indicates the improvement gained over UDD at that time. Note the log scale. The blue line with vertical dashes represents a LODD simulation adjusting the pulse timings to give optimum error suppression at each point along the curve. It shows an improvement of at least an order of magnitude over UDD at most times. The timing of each pulse sequence (relative to each corresponding total free evolution time) is shown in (b) on the same time axis. The dotted lines in (b) show the pulse timings of the UDD sequence. The horizontal dashed line in (a) indicates the current detection threshold of our system. In all cases the same ohmic spectrum with a sharp cutoff around 500 Hz was used.

simulation, accurate knowledge of the relevant noise spectrum is required. An alternative is to use measurement feedback as input to the Nelder-Mead algorithm, rather than theoretical calculation of the coherence signal from Eq. (5).

Figure 5(a) compares the performance of one such LODD sequence to UDD and CPMG. The LODD sequence (green squares) was optimized for the free-evolution time $\tau = 2.4$ ms and we see that it achieves an improved fidelity over that of UDD (black triangles) by a factor of 4.7, at that time. This sequence was obtained using measurement feedback, illustrating that the optimization approach can be effectively used even without prior knowledge of the noise spectrum in a system.

To obtain optimum error suppression over the whole range of free-evolution times, it is necessary to find an optimized pulse sequence for *each* τ. In this way we obtain (in this case by simulation) the blue line with vertical dashes in Fig. 5(a), showing that such an LODD sequence outperforms UDD by an order of magnitude, or more, over almost the entire range of free-evolution times. We plot in Fig. 5(b) the LODD timing sequence obtained at each τ that leads to the corresponding point in the LODD curve in Fig. 5(a).

In the high fidelity regime a large fraction of the LODD curve lies below our current detection threshold. The ability of the theory to reproduce fine features of our data in the lower fidelity regime, as seen in Fig. 4(a)-(b), suggests similar agreement will be obtained in the high fidelity regime with some improvements to our measurement system. In particular we anticipate measuring at the 10^{-3} level by eliminating sources of stray laser light and by aperturing the fluorescence detecting photo-tube.

6. CONCLUSION

In this study we compared the phase-noise suppression efficiency of the recently proposed UDD sequence to that of the traditional CPMG technique. As predicted by theoretical treatments, we found that UDD outperforms the CPMG approach in an ohmic spectrum with a high-frequency cutoff, while it performs similarly to CPMG in a noise spectrum with a soft $1/\omega^4$ roll-off. In addition, we demonstrated that further improvements can be made by finding a pulse sequence that gives optimum error suppression for each total free-evolution time of the qubit, i.e., locally optimized dynamical decoupling sequences. The gains over traditional NMR techniques reported here, suggest that judiciously chosen decoupling sequences are indeed promising candidates for mitigating the effects of decoherence on quantum information processing, in systems where the noise spectrum allows such gains, i.e., systems with noise spectra having sharp, high-frequency cutoffs.

An optimization strategy that we did not consider, but can potentially develop the capability to implement, entails shaping the microwave π-pulses to have smooth time-varying amplitudes, as opposed to the square pulses used in our system. Recent studies indicate that appropriate choice of the pulse envelope alone can lead to significant error suppression.[14, 15] Combining strategies such as the latter and that discussed in this paper will most likely provide enhanced error suppression to any single approach alone.

REFERENCES

[1] Hahn, E., "Spin echoes," *Phys. Rev.* **80**, 580–594 (1950).

[2] Knill, E., Laflamme, R., and Zurek, W. H., "Resilient quantum computation: Error models and thresholds," *Math., Phys. and Eng. Sci.* **454**, 365–384 (1998).

[3] Aliferis, P., Gottesman, D., and Preskill, J., "Accuracy threshold for postselected quantum computation," *Quant. Info. and Comp.* **8**, 181–244 (2008).

[4] Viola, L. and Lloyd, S., "Dynamical suppression of decoherence in two-state quantum systems," *Phys. Rev. A* **58**, 2733 (1998).

[5] Viola, L., Knill, E., and Lloyd, S., "Dynamical decoupling of open quantum systems," *Phys. Rev. Lett.* **82**, 2417 (1999).

[6] Khodjasteh, K. and Lidar, D., "Fault-tolerant quantum dynamical decoupling," *Phys. Rev. Lett.* **95**, 180501 (2005).

[7] Uhrig, G., "Keeping a quantum bit alive by optimized π-pulse sequences," *Phys. Rev. Lett.* **98**, 100504 (2007).

[8] Uhrig, G., "Exact results on dynamical decoupling by π pulses in quantum information processes," *New Journal of Physics* **10**, 083024 (2008).

[9] Cywinski, L., Lutchyn, R., Nave, C., and Sarma, S. D., "How to enhance dephasing time in superconducting qubits," *Phys. Rev. B* **77**, 174509 (2008).

[10] Vandersypen, L. and Chuang, I., "Nmr techniques for quantum control and computation," *Rev. Mod. Phys.* **76**, 1037 (2004).

[11] Lee, B., Witzel, W., and Sarma, S. D., "Universal pulse sequence to minimize spin dephasing in the central spin decoherence problem," *arxiv.org 0710.1416* (2008).

[12] Jensen, M., Hasegawa, T., and Bollinger, J., "Temperature and heating rate of ion crystals in penning traps," *Phys. Rev. A* **70**, 033401 (2004).

[13] Press, W., Teukolsky, S., Vetterling, W., and Flannery, B., [*Numerical recipes : the art of scientific computing, 3rd ed*], Cambridge University Press, New York (2007).

[14] Shiokawa, K. and Lidar, D., "Dynamical decoupling using slow pulses: Efficient suppression of 1/f noise," *Phys. Rev. A* **69**, 030302(R) (2004).

[15] Pasini, S., Fischer, T., Karbach, P., and Uhrig, G., "Optimization of short coherent control pulses," *Phys. Rev. A* **77**, 032315 (2008).